



# Why Do Chromospheric Oscillations in Sunspot Umbrae Appear to Propagate Downward?

Jongchul Chae<sup>1,3</sup> , Eun-Kyung Lim<sup>2</sup> , Kyeoree Lee<sup>1</sup> , Hannah Kwak<sup>2</sup> , Kyoung-Sun Lee<sup>1</sup> , Juhung Kang<sup>1</sup> , and Soosang Kang<sup>1</sup> 

<sup>1</sup> Astronomy Program, Department of Physics and Astronomy, Seoul National University, Gwanak-gu, Seoul 08826, Republic of Korea; [jcchae@snu.ac.kr](mailto:jcchae@snu.ac.kr)

<sup>2</sup> Solar and Space Weather Group, Korea Astronomy and Space Science Institute, Daejeon 34055, Republic of Korea

Received 2022 October 8; revised 2023 February 2; accepted 2023 February 8; published 2023 February 22

## Abstract

Umbral oscillations constitute the most noticeable chromospheric feature of sunspot umbrae—large-amplitude oscillations of intensity (umbral flashes, if very strong) and line-of-sight velocity, with periods of about 3 minutes. These umbral oscillations are usually interpreted as acoustic waves propagating upward under the effect of gravity. However, there have been observational reports that intensity peaks tend to occur in downflowing phases of umbral oscillations, and this appears to be more compatible with downward propagation. We investigate whether this intensity–velocity correlation occurs persistently or not, by determining the vertical flux of the wave energy, based on  $H\alpha$  line measurements of the temperature and velocity. As a result, we find that the wave flux is persistently negative in sunspot umbrae, confirming the discrepancy specified above. We attribute this discrepancy to the nonzero fluctuation of net radiative heating. We find that when this effect is taken into account in the energy equation, the pressure is peaked during upflowing phases, being compatible with the notion of upward propagation. We conclude that temperature (and intensity) peaks occur during downflowing phases, not because of downward propagation, but because of radiative heat transport.

*Unified Astronomy Thesaurus concepts:* Sunspots (1653); Magnetohydrodynamics (1964); Solar chromosphere (1479)

## 1. Introduction

The chromosphere of a sunspot umbra is always dynamic, in that both the intensity of a strong spectral line and the line-of-sight velocity inferred from that line ceaselessly oscillate at periods of about 3 minutes, with large amplitudes (Beckers & Tallant 1969; Giovanelli 1972). A series of earlier studies (Lites 1984; Centeno et al. 2006; Felipe et al. 2010) have investigated the phase difference between the oscillations, measured with a pair of spectral lines, and concluded that the umbral oscillations propagate upward. This notion of upward propagation has been questioned by other studies on the correlation between the intensity and velocity of a strong absorption line. It was recently found that an intensity increase occurs during the downflowing phase in the umbral oscillations of a small sunspot (Lites et al. 1982; Cho et al. 2015) as well as the umbral flashes of large sunspots (Henriques et al. 2017; Bose et al. 2019). This kind of intensity–velocity correlation appears to be consistent with the notion of downward propagation. On the other hand, recent numerical simulations of umbral flashes (Felipe et al. 2021) have indicated that the umbral flashes are upflowing most of time and that downflowing umbral flashes are shorter-lived, in agreement with the standing waves in sunspot umbrae. It is necessary, then, to observationally verify whether the reported brightening–downflow correlation occurs transiently for shorter durations or persistently for longer durations, in each period of oscillation.

The strategy that we adopt in the present work involves inferring not only the vertical velocity fluctuation, but also the temperature fluctuation, from the  $H\alpha$  line. We then determine the vertical flux of the wave energy from these fluctuations, by assuming that the waves are adiabatic. If the temperature is positively correlated with the upward (downward) velocity, the wave flux is found to be positive (negative), and the fluctuations apparently represent upward (downward)–propagating waves. Since the correlation between the temperature and the velocity may fluctuate with phase, we examine the 3 minute running average of the wave flux or its average over a longer time interval.

In the present work, we first show that the negative wave flux is really persistent in sunspot umbrae, indicating that a temperature increase (as well as an intensity increase) commonly occurs during the downflowing phase, apparently going against the widely accepted notion of upward propagation. Next, we show that this discrepancy may be due to the nonadiabatic nature of the waves, and that it can be resolved if the nonadiabatic effect of the radiative energy transport is properly taken into account.

## 2. Method and Data

Umbral oscillations are regarded as the observed signatures of slow magnetoacoustic waves in sunspot umbrae (e.g., Khomenko & Collados 2015). In sunspot umbrae, the plasma  $\beta$  is close to unity near the photosphere and much smaller than unity in the chromosphere. The slow magnetoacoustic waves in the umbral chromosphere may be fairly approximated by 1D acoustic waves under the effect of gravity. The vertical flux of

<sup>3</sup> Corresponding author.

the wave energy is given by

$$F = \frac{\gamma}{\gamma - 1} p v, \quad (1)$$

with the pressure  $p$ , the vertical velocity  $v$  (positive upward), and the specific heat ratio  $\gamma$ . As a working hypothesis, we assume that the acoustic waves are adiabatic. With the initially undisturbed values of the pressure  $p_0$  and temperature  $T_0$ , we then obtain

$$p = p_0 \left( \frac{T}{T_0} \right)^{\frac{\gamma}{\gamma-1}}, \quad (2)$$

expressed in terms of the temperature  $T$ :

$$F = \frac{\gamma}{(\gamma - 1)} p_0 \left( \frac{T}{T_0} \right)^{\frac{\gamma}{\gamma-1}} v. \quad (3)$$

In the limit when the fluctuation amplitudes are small, the above expression is reduced to the linear version:

$$F = \frac{\gamma^2}{(\gamma - 1)^2} p_0 \frac{T - T_0}{T_0} v. \quad (4)$$

The important point is that the direction of the wave propagation is completely determined by the sign of  $F$  or by that of  $(T - T_0)v$  in the linear limit. The above expressions are particularly useful from the observer's point of view, because both  $v$  and  $T$  can be measured from observations. Since the fluctuation amplitudes are found to be large enough, we do not use this linear version, and stick to the nonlinear version in Equation (7).

Basically,  $v$  and  $T$  are inferred from the center wavelength and the Doppler width, respectively, of the  $H\alpha$  absorption profile in the chromosphere. Because of the light mass of hydrogen, thermal broadening dominates the broadening of the  $H\alpha$  absorption profile. After the much smaller contribution of the nonthermal broadening has been subtracted, by making use of the Doppler width of the simultaneously recorded Ca II 8542 line (Park et al. 2013), the Doppler width of the  $H\alpha$  line yields a quite reasonable estimate of  $T$  (e.g., Chae et al. 2021).

The physical parameters are inferred from the  $H\alpha$  line profile and the Ca II 8542 line profile, using the technique of multilayer spectral inversion (MLSI; Chae et al. 2020, 2021). In MLSI, the atmosphere is assumed to consist of three layers: the upper chromospheric layer, forming the core part of the line; the lower chromospheric layer, forming the wing part of the line; and the photosphere, forming the far wing and the continuum. In each layer, each of the source function, the line-of-sight velocity, and the Doppler width vary with optical depth, with a constant gradient. The model of a line profile is then characterized by a total of 17 parameters, including 10 free parameters that are determined from the constrained fitting of the observed line profile (Chae et al. 2021). Most important among the 10 free parameters are the parameters describing the upper chromosphere: the source function  $S_r$ , the line-of-sight velocity  $v_r$ , and the Doppler width  $w_r$  at the top of this layer, as well as the corresponding parameters  $S_b$ ,  $v_b$ , and  $w_b$  at the bottom of this layer. The vertical velocity  $v$  used for the present study comes from  $v_r$  of the  $H\alpha$  line, and the temperature  $T$  is determined from  $w_r$  of the same line, with the nonthermal contribution to  $w_r$  being subtracted by making use of the value of  $w_r$  of the Ca II 8542 line, as explained by Chae et al. (2021).

The line core intensity  $I$  is identified with  $S_r$ , the source function at the top of the upper chromosphere. This intensity is not subject to the Doppler effect, unlike the line intensity measured at a fixed wavelength. We express the intensity in units of continuum intensity  $I_0$  around the spectral line and as measured in quiet regions at the solar disk center.

It has to be admitted that the determination of the temperature from the  $H\alpha$  line has not been fully established yet. Most of all, this line is a strongly scattering line, so the non-local thermodynamic equilibrium solution of radiative transfer requires full 3D modeling (Leenaarts et al. 2012). Our MLSI analysis evades this formidable task, by treating the values of the source function as model parameters to be determined from observations. The validity of using the Doppler width of the  $H\alpha$  line as a temperature diagnostic is supported by the observed strong correlation between the intensity of the Atacama Large Millimeter/submillimeter Array (ALMA) and the width of the  $H\alpha$  line (Molnar et al. 2019). However, a discrepancy was noticed as well; the amplitude of the temperature fluctuation from the  $H\alpha$  observations was usually larger than that from ALMA. In the present study, we have found the amplitudes of the  $H\alpha$  temperature fluctuations from umbral oscillations to be as large as 3000 K, which is much larger than the 500 K inferred from ALMA observations (Chai et al. 2022). One might attribute this discrepancy to the increase of the  $H\alpha$  width, by either the complex response function of the line (e.g., Socas-Navarro & Uitenbroek 2004) or the phase-dependent change of its formation height, due to the opacity effect (Molnar et al. 2019; Felipe & Socas-Navarro 2023). The full resolution of this discrepancy is much beyond the present work, but we think that the temperature fluctuations of large amplitude are not physically unrealistic in highly nonlinear umbral oscillations. The temperature fluctuations can be as large as a few tenths of the undisturbed temperature, when the velocity amplitude is comparable to the local sound speed.

Specifically, we use data taken from a small sunspot (pore) in AR 12078, observed near the disk center on 2014 June 3 using the Fast Imaging Solar Spectrograph (FISS) of the 1.6 m Goode Solar Telescope (GST) at the Big Bear Solar Observatory. The observations yielded a time series of raster scans of the  $H\alpha$  line spectra and the Ca II 8542 line spectra at a cadence of 20 s. This set of observations has previously been used for the study of the waves in the sunspot (Chae et al. 2015; Kang et al. 2019), but it has never been used for the determination of the wave flux, based on temperature measurements.

We have determined the vertical velocity  $v$  and the temperature  $T$  at every spatial pixel and every instant of the measurements. The undisturbed value  $T_0$  at a location is identified with the average of  $T$  over all the measurements there. We have suppressed noises and low-frequency variations by applying the bandpass filter between 1 and 4 minutes to the time series of the velocity  $v$  and temperature fluctuations  $\delta T \equiv T - T_0$  at every location. Note that the vertical velocity  $v$  is defined to be positive if motion is upward, so upward-propagating waves have  $v\delta T > 0$ . We choose  $\gamma = 5/3$ , by neglecting the effects of hydrogen ionization/recombination (see, e.g., Carlsson & Stein 2002), and  $p_0 = 1.2 \text{ dyn cm}^{-2}$ , the gas pressure at the supposed  $H\alpha$  formation height of 1500 km in the umbral core model M of Maltby et al. (1986).

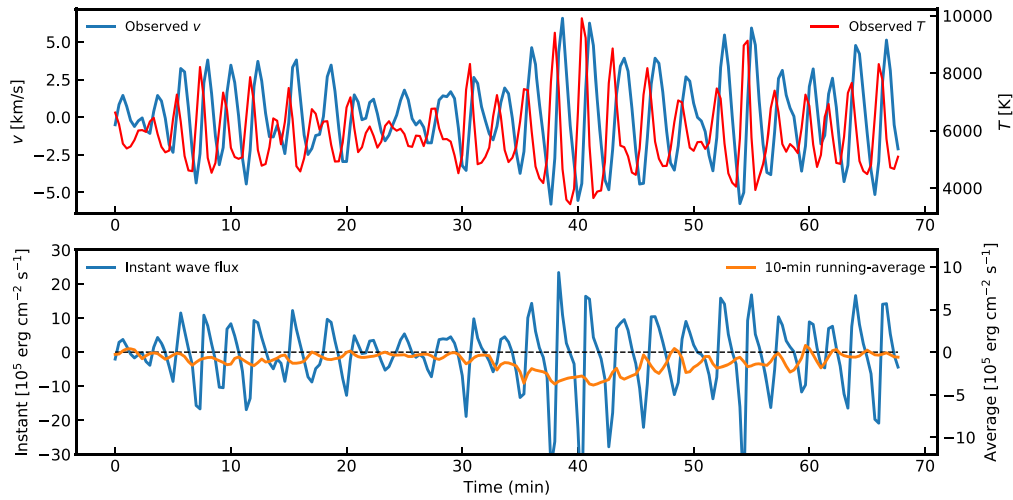


**Figure 1.** Top: time variations of the observed vertical velocity and observed temperature, inferred from the  $H\alpha$  line spectra taken at a location inside a sunspot umbra. Bottom: time variations of the wave energy flux calculated from the observed vertical velocity and observed temperature, and the 10 minute running average.

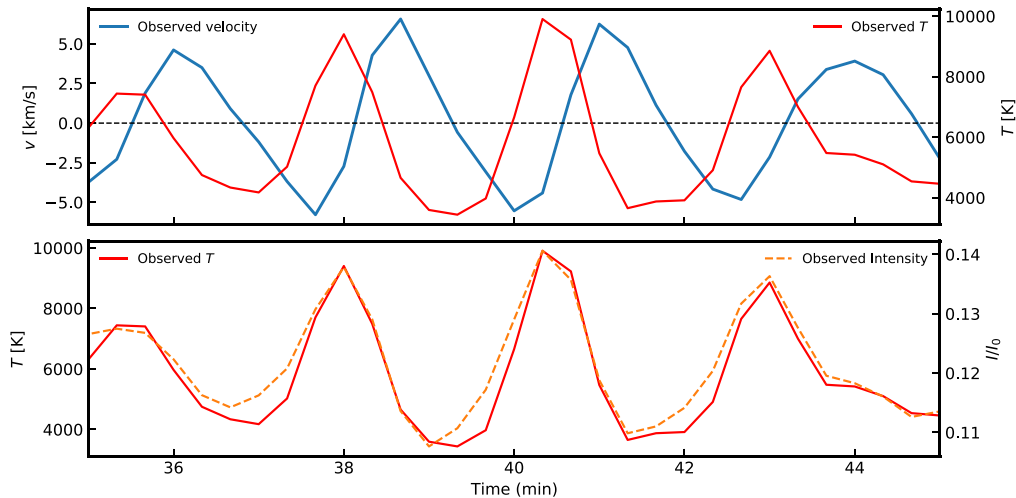


**Figure 2.** Top: enlarged plots of the vertical velocity and temperature of the  $H\alpha$  line during a time interval. Bottom: plots of the temperature and the line core intensity.

### 3. Results

The top panel of Figure 1 illustrates the temporal variations of velocity and temperature in the chromosphere at a specific location of the sunspot umbra. We find that the velocity fluctuates with amplitudes  $v_1$  as large as  $6.6 \text{ km s}^{-1}$ , while the temperature fluctuates from 3440 to 9900 K with a mean of  $T_0 = 5880 \text{ K}$ . The bottom panel of Figure 1 shows the variation of the wave flux  $F$ , determined from  $v$  and  $T$  using Equation (3). We find that even though  $F$  fluctuates between positive values and negative values, the negative values have larger amplitudes than the positive values. As a result, the running average of  $F$  over 10 minutes is found to be negative all the times. Specifically, the 10 minute running average at a time of 40 minutes is estimated as  $-2.9 \times 10^5 \text{ erg cm}^{-2} \text{ s}^{-1}$ .

The negative wave flux is attributed to the phase difference between velocity and temperature, as is well seen from the top panel of Figure 2. The temperature fluctuation precedes the velocity fluctuation, with the temperature peak occurring at the downflowing phase, when the velocity is still negative. This finding is consistent with the previous finding that the brightening in umbral oscillations or umbral flashes occurs in the downflow phase. The data plotted in the bottom panel of Figure 2 indicate that the intensity fluctuates fully in phase with

the temperature, supporting the notion that the intensity fluctuation is due to the temperature fluctuation.

We find that the behavior of the negative average wave flux is dominant inside sunspot umbrae. Figure 3 clearly illustrates this characteristic. As is very well known, the figure confirms that in the umbra, the velocity fluctuates with large amplitudes. It also shows that the temperature fluctuates as well, in agreement with the compressive nature of umbral oscillations. Moreover, the maps of velocity and temperature suggest that the velocity fluctuations and the temperature fluctuations are correlated with each other. In the area surrounding the marked position, the velocity is negative (downward motion) and the temperature is positively enhanced at the specified instant, suggesting that the wave flux is negative in this area at this instant. In fact, the wave flux, when averaged over a long time interval, is found to be negative almost everywhere inside the umbra, as is shown in the bottom panel of Figure 3. A comparison of the two maps showing the time-averaged flux indicates that the spatial distribution of the time-averaged flux changes a little with time, with their signs remaining negative at most points inside the umbra.

The sunspot used for our study is a pore near the disk center—a small sunspot without a white-light penumbra. We choose

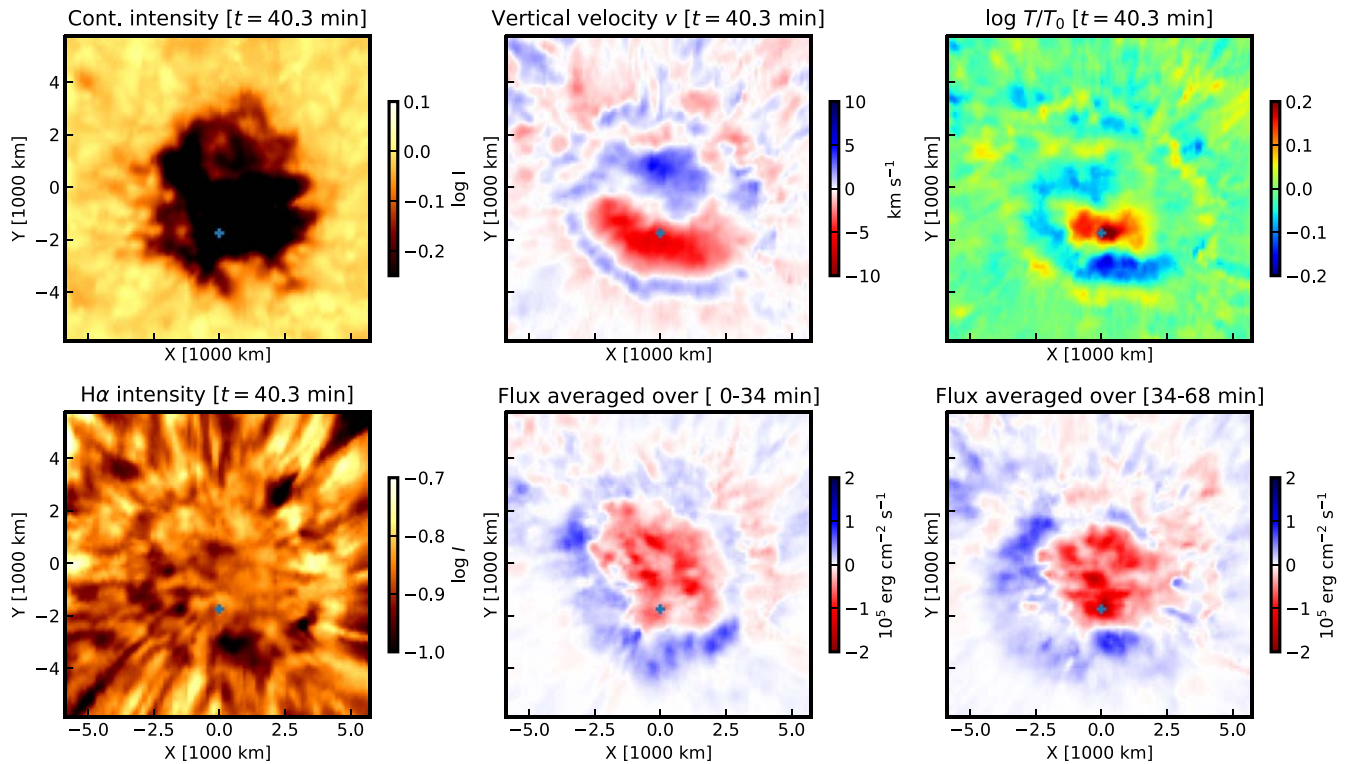


**Figure 3.** Maps of the continuum intensity (top left), vertical velocity (top middle), temperature fluctuation (top right), and  $H\alpha$  core intensity (bottom left) of the sunspot constructed at a specific instant ( $t = 40.3$  minutes), as well as the mean wave flux of the first 34 minutes (bottom middle) and that of the second 34 minutes (bottom right). The symbol marks the location from where the data plotted in Figures 1, 2, 4, 5, and 6 are taken.

this sunspot for demonstration simply because the FISS data taken from this sunspot are excellent. We have examined other large sunspots as well (including the main spot of the McIntosh class Cso observed on the disk on 2014 June 3, the leading sunspot of the McIntosh class Dai in AR 12715 observed near the disk center on 2018 June 21, and the trailing sunspot of the McIntosh class Dao in AR 12715 observed near disk center on 2018 June 22) and confirmed that the wave flux is apparently negative in these sunspot umbrae, irrespective of the sunspot type and development stage. Note that this conclusion, however, has limitations. It is valid only for the layer where the  $H\alpha$  line is formed, and only under the assumption of adiabatic waves.

#### 4. Discussion

We have found that the wave flux determined from  $v$  and  $T$  as inferred from the  $H\alpha$  line is persistently negative in sunspot umbrae. We have also confirmed that the intensity fluctuation is strongly and positively correlated with the temperature fluctuation. Therefore, our result indicates that the previously reported occurrence of intensity peaks during the downflowing phase (Lites et al. 1982; Cho et al. 2015; Henriques et al. 2017; Bose et al. 2019; Yurchyshyn et al. 2020) is quite a persistent phenomenon in umbral oscillations and umbral flashes.

The persistency of the negative wave flux that we have found would be quite surprising if it could be interpreted as evidence of the downward propagation of umbral oscillations. This goes against the results of previous studies indicating that chromospheric umbral oscillations represent upward-propagating waves. The first kind of observational evidence for upward propagation came from an investigation of the phase difference between the velocity variations determined from a photospheric

spectral line and those from a chromospheric spectral line (Lites 1984; Centeno et al. 2006; Felipe et al. 2010). Further evidence came from the positive correlation between the upward motion and brightening that was observed in UV emission lines that were emitted from the transition region (Brynildsen et al. 1999; Tian et al. 2014). This is opposite to the correlation of the intensity and velocity that we see in the  $H\alpha$  line, and supports the upward propagation of the umbral oscillations in the transition region. Meanwhile, the upward-propagating nature of umbral oscillations throughout the chromosphere and low corona has been indicated by the observed delays in coronal flashes in comparison with the chromospheric flashes inferred from Solar Dynamics Observatory/Atmospheric Imaging Assembly observations (Sych & Nakariakov 2014). Finally, the apparent horizontal propagation of the oscillation patterns seen in umbrae at different atmospheric levels has been successfully explained by the time difference in waves propagating upward along different magnetic waveguides from the photosphere (Zhao et al. 2015; Cho et al. 2019; Kang et al. 2019; Cho & Chae 2020).

With all of these observations being taken into account, we conclude that the persistency of the negative wave flux observed from the  $H\alpha$  line may not imply that the umbral oscillations propagate downward. What, then, is the reason for this discrepancy? Why do chromospheric umbral oscillations appear to propagate downward, even if they do not?

We think that the discrepancy originates from the assumption of adiabatic waves, where the pressure is supposed to fluctuate in phase with the temperature. In nonadiabatic waves, however, there may be a phase difference between the pressure fluctuation and the temperature fluctuation, because of the nonzero fluctuation of the net heating rate  $\delta Q$ , as can be seen

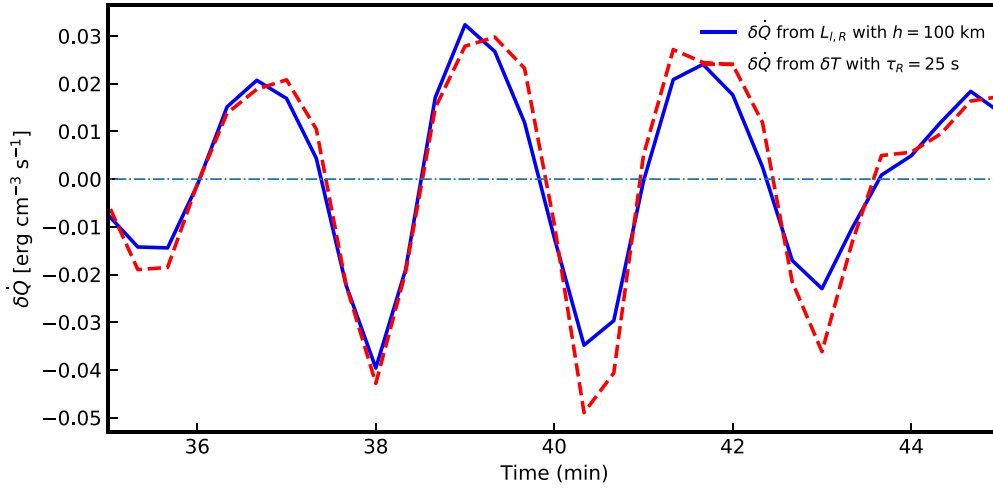


**Figure 4.** Time variations of  $\delta\dot{Q}$  determined from  $L_{l,R}$  and  $\delta T$ , respectively, with the values of  $T_0 = 5880$  K,  $p_0 = 1.2$  dyn cm $^{-2}$ , and  $\gamma = 1.67$ .

from the internal energy equation (e.g., Priest 2014):

$$\frac{p}{\gamma - 1} \frac{d}{dt} \ln \frac{p}{\rho^\gamma} = \delta\dot{Q}. \quad (5)$$

With the help of the condition  $p \propto \rho T$ , we solve the above equation for  $p$ :

$$p = p_0 \left( \frac{T}{T_0} \right)^{\frac{\gamma}{\gamma-1}} \exp(-\Psi), \quad (6)$$

which is inserted into Equation (1), to obtain:

$$F = \frac{\gamma}{(\gamma - 1)} p_0 \left( \frac{T}{T_0} \right)^{\frac{\gamma}{\gamma-1}} \exp(-\Psi) v, \quad (7)$$

with

$$\Psi \equiv \int^t \frac{\delta\dot{Q}}{p} dt \approx \frac{1}{\langle p \rangle} \int^t \delta\dot{Q} dt. \quad (8)$$

Note that at each location, the average  $\langle \rangle$  is taken over all the measurements and the constant of integration for  $\Psi$  is set to the value that ensures  $\langle \Psi \rangle = 0$ .

We attribute nonzero  $\delta\dot{Q}$  to the net radiative heating. According to our observations, a temperature peak precedes a velocity peak. This observed property suggests that there may be a process transmitting the temperature fluctuations earlier than the velocity fluctuations. It is very likely that the radiative transport of heat is such a process. We also note that there may be some contribution to  $\dot{Q}$  from irreversible heating, such as shock heating, because the oscillations in the upper chromosphere are nonlinear. This effect, however, is not taken into account in our study, for simplicity.

There are two ways to specify  $\delta\dot{Q}$ . First, we specify  $\delta\dot{Q}$  using the line radiative loss  $L_{l,R} \equiv F_{l,t} - F_{l,b}$ , where  $F_{l,t}$  is the radiative flux at the top of the upper chromosphere integrated over the H $\alpha$  line and  $F_{l,b}$  is that at the bottom. By adopting the plane-parallel assumption, we obtain the expression

$$\delta\dot{Q} = -\frac{\alpha \delta L_{l,R}}{\Delta z} = -\frac{\delta L_{l,R}}{h}, \quad (9)$$

where  $\Delta z$  is the geometrical thickness of the upper chromosphere, and the numeric parameter  $\alpha$  is the ratio of the radiative flux integrated over the line to the total radiative flux over all

the spectral lines, including the Mg II lines and Ca II lines. For convenience, we assume that  $h \equiv \Delta z / \alpha$  is a constant parameter of our model. Note that  $F_{l,t}$  and  $F_{l,b}$  can be completely determined using the expression of radiation flux in a plane-parallel atmosphere and the MLSI parameters of the line at every location and every instant. Second, we specify  $\delta\dot{Q}$  using Newton's cooling law (e.g., Mihalas & Mihalas 1984), as in

$$\delta\dot{Q} = -\frac{p_0}{(\gamma - 1) T_0} \frac{\delta T}{\tau_R}, \quad (10)$$

with the radiative relaxation time  $\tau_R$ .

In our observations, the mean radiative loss  $L_{l,R}$  is estimated as  $0.91 \times 10^6$  erg s $^{-1}$  cm $^{-2}$ , which is much smaller than the reported total radiative loss—for example,  $4.5$  to  $108 \times 10^6$  erg s $^{-1}$  cm $^{-2}$ , as obtained from an active region by Díaz Baso et al. (2021). The amplitude of the fluctuating radiative loss  $\delta L_{l,R}$  during the time interval between 36 and 42 minutes is estimated as  $0.27 \times 10^6$  erg s $^{-1}$  cm $^{-2}$ , which is also much smaller than the reported amplitude of the total radiative loss fluctuation—for example,  $7.6 \times 10^6$  erg s $^{-1}$  cm $^{-2}$ , as obtained from a plage region by Morosin et al. (2022). The big difference between our estimates and the other estimates may be partly attributed to the small value of  $\alpha$ , the ratio of the H $\alpha$  radiative loss to the total radiative loss.

Figure 4 shows the time variations of  $\delta\dot{Q}$  that we calculated using Equations (9) and (10), respectively. To calculate  $\delta\dot{Q}$  in Equation (9) from  $\delta L_{l,R}$ , we have chosen  $h = 100$  km, for illustration. We also select a set of  $\tau_R$  to see the variation of  $\delta\dot{Q}$  in Equation (10). Interestingly, with the choice of  $\tau_R = 25$  s, we could make the two plots match each other fairly well. This suggests that the commonly used approach of Newton's law is quite a good approximation for the net radiative heating by the H $\alpha$  line. In other words, it suggests that as far as the net radiative heating is concerned, the H $\alpha$  can be considered to be effectively optically thin. For our analysis, we have assumed that the total net radiative heating by all the spectral lines, including the Mg II h and k lines and the Ca II H and K lines, is proportional to the net radiative heating by H $\alpha$ . As a matter of fact, the effectively optically thin approximation in these lines of Mg II and Ca II may not be as valid as for the H $\alpha$  line. This problem has to be investigated in the future, for a more rigorous treatment of the total net radiative heating.

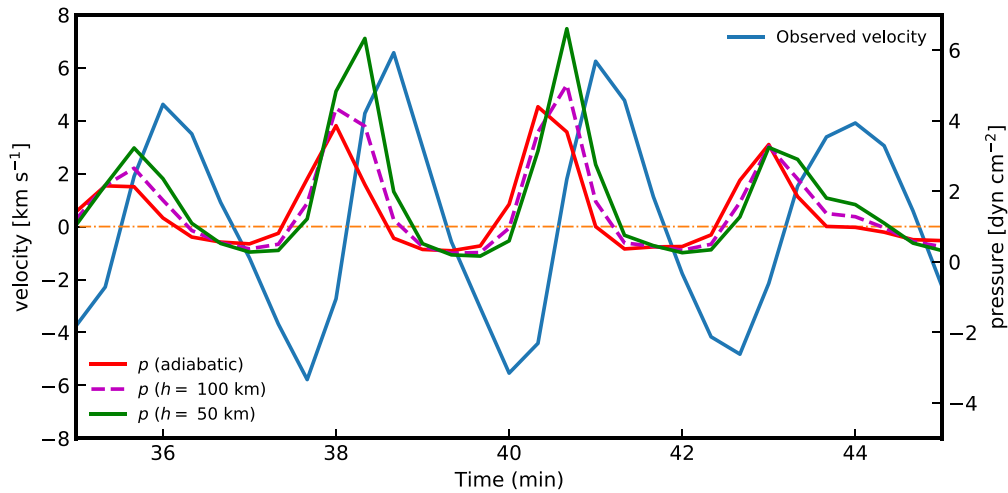


**Figure 5.** Time variations of  $p$  calculated from  $T$  and  $L_{i,R}$ , by taking into account the fluctuation of the radiative heating/cooling in a few cases of  $h$ .

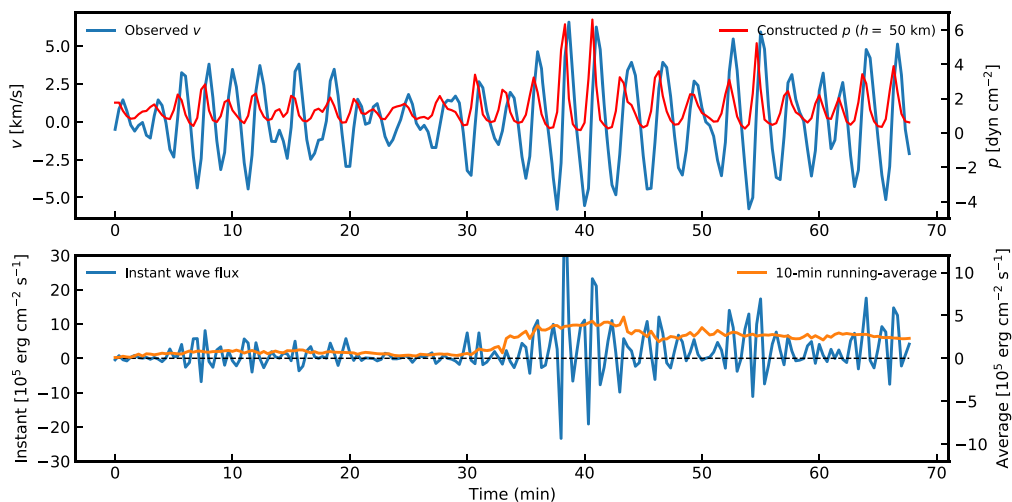


**Figure 6.** Top: time variations of  $p$  and  $v$  over the whole observing time. Bottom: time variations of the wave flux and running averaged wave flux.

Figure 5 shows the time variation of  $p$  determined using Equation (6). In our study,  $h = 100$  km and  $50$  km correspond to  $\tau_R = 25$  s and  $12.5$  s, respectively. Note that these values of  $\tau_R$  are compatible with the values that have previously been determined from the comparison of the oscillation phases between two different lines in each pair (Centeno et al. 2006; Felipe et al. 2010), but are significantly smaller than  $143$  s, the value at the chromospheric height of  $810$  km that was theoretically calculated by Souffrin (1972), using the assumption of local thermodynamic equilibrium. Under the adiabatic assumption (zero net radiative heating),  $T$  and  $p$  vary in phase with each other. However, when the net radiative heating is not zero, the variations of  $T$  and  $p$  are not in phase with each other. As we expect, the peak of  $p$  occurs later than the peak of  $T$ . For a given variation of  $T$ , the phase difference is found to be bigger as the contribution of the radiative effect becomes larger (with  $h$  being smaller). If this contribution is large enough, the peak of  $p$  occurs during the upflowing ( $v > 0$ ) phase, in agreement with the upward wave propagation. Moreover, the peak of  $p$  becomes higher for larger radiative contributions, suggesting a larger upward wave flux.

Figure 6 shows the time variation of  $p$ , constructed with  $h = 50$  km over the whole observing time, in comparison with  $v$  and the time variation of the wave flux using Equation (7). It is

clear from the figure that the wave flux is persistently positive, with the running averaged wave flux always being positive, in contrast with Figure 1. The running average wave flux at the time of  $40$  minutes is estimated as a positive value,  $3.9 \times 10^5$  erg cm $^{-2}$  s $^{-1}$  ( $h = 50$  km), which is contrasted with the negative value of  $-3.3 \times 10^5$  erg cm $^{-2}$  s $^{-1}$  determined above. This means that the wave fluxes appear to be negative when the waves are assumed to be adiabatic, but are found to have positive fluxes when the net radiative heating is properly taken into account in the energy equation. The net radiative heating makes the temperature peak occur earlier than the pressure peak, so that the temperature peak may occur during the downflowing phase, whereas the pressure peak occurs during the upflowing phase. Thus, the discrepancy noticed above has now been fully resolved. Note that this analysis has been performed at one location inside the umbra, for illustration. A similar analysis can be performed for umbral oscillations at other locations as well, if  $h$  is given.

## 5. Conclusion

During umbral oscillations, both the velocity and temperature fluctuate in time with large amplitudes. We have found that temperature enhancement (and hence brightening as well)

occurs persistently during the downflowing phase in the atmospheric level, seen through the core of the  $H\alpha$  line. Under the assumption of adiabatic waves, this finding could be interpreted as evidence for the downward propagation of umbral oscillations, going against the widely accepted notion of upward propagation. This discrepancy can be resolved when the fluctuation of the net radiative heating rate is properly taken into account. Allowing the effects of net radiative heating, pressure enhancement is found to occur during the upflowing phase, being compatible with upward propagation. Our study indicates that a proper treatment of the net radiative heating is crucial for the determination of the acoustic wave flux in chromospheric umbral oscillations. For a reasonable estimate of the wave flux, it will be necessary to determine the value of the free parameter ( $h$  or  $\tau_R$ ) well. These values may vary, depending on the observed region, because of the dependence of the radiative transfer on the atmospheric structure.

We would like to thank the referee for a careful manuscript reading, constructive comments, and insightful suggestions. This research was supported by the National Research Foundation of Korea (NRF-2020R1A2C2004616 and NRF-2021R1A2C1010881). E.-K.L. was supported by the Korea Astronomy and Space Science Institute, under the R&D program supervised by the Ministry of Science and ICT. The GST operation is partly supported by the Korea Astronomy and Space Science Institute, the Seoul National University, the Key Laboratory of Solar Activities of the Chinese Academy of Sciences (CAS), and the Operation, Maintenance and Upgrading Fund of CAS for Astronomical Telescopes and Facility Instruments.

#### ORCID iDs

Jongchul Chae  <https://orcid.org/0000-0002-7073-868X>  
 Eun-Kyung Lim  <https://orcid.org/0000-0002-7358-9827>  
 Kyeoree Lee  <https://orcid.org/0000-0001-9455-3615>  
 Hannah Kwak  <https://orcid.org/0000-0001-8619-9345>  
 Kyoung-Sun Lee  <https://orcid.org/0000-0002-4329-9546>  
 Juhung Kang  <https://orcid.org/0000-0003-3540-4112>  
 Soosang Kang  <https://orcid.org/0000-0002-3657-4845>

#### References

- Beckers, J. M., & Tallant, P. E. 1969, *SoPh*, **7**, 351  
 Bose, S., Henriques, V. M. J., Rouppe van der Voort, L., et al. 2019, *A&Ap*, **627**, A46  
 Brynildsen, N., Kjeldseth-Moe, O., Maltby, P., et al. 1999, *ApJL*, **517**, L159  
 Carlsson, M., & Stein, R. F. 2002, *ApJ*, **572**, 626  
 Centeno, R., Collados, M., & Trujillo Bueno, J. 2006, *ApJ*, **640**, 1153  
 Chae, J., Cho, K., Kang, J., et al. 2021, *JKAS*, **54**, 139  
 Chae, J., Madjarska, M. S., Kwak, H., et al. 2020, *A&Ap*, **640**, A45  
 Chae, J., Song, D., Seo, M., et al. 2015, *ApJL*, **805**, L21  
 Chai, Y., Gary, D. E., Reardon, K. P., et al. 2022, *ApJ*, **924**, 100  
 Cho, K., & Chae, J. 2020, *ApJL*, **892**, L31  
 Cho, K., Chae, J., Lim, E. k., et al. 2019, *ApJ*, **879**, 67  
 Cho, K.-S., Bong, S.-C., Nakariakov, V. M., et al. 2015, *ApJ*, **802**, 45  
 Díaz Baso, C. J., de la Cruz Rodríguez, J., & Leenaarts, J. 2021, *A&A*, **647**, A188  
 Felipe, T., Henriques, V. M. J., de la Cruz Rodríguez, J., et al. 2021, *A&Ap*, **645**, L12  
 Felipe, T., Khomenko, E., Collados, M., & Beck, C. 2010, *ApJ*, **722**, 131  
 Felipe, T., & Socas-Navarro, H. 2023, arXiv:2301.03273  
 Giovanelli, R. G. 1972, *SoPh*, **27**, 71  
 Henriques, V. M. J., Mathioudakis, M., Socas-Navarro, H., & Rodríguez, J. d. I. C. 2017, *ApJ*, **845**, 102  
 Kang, J., Chae, J., Nakariakov, V. M., et al. 2019, *ApJL*, **877**, L9  
 Khomenko, E., & Collados, M. 2015, *LRSP*, **12**, 6  
 Leenaarts, J., Carlsson, M., & Rouppe van der Voort, L. 2012, *ApJ*, **749**, 136  
 Lites, B. W. 1984, *ApJ*, **277**, 874  
 Lites, B. W., White, O. R., & Packman, D. 1982, *ApJ*, **253**, 386  
 Maltby, P., Avrett, E. H., Carlsson, M., et al. 1986, *ApJ*, **306**, 284  
 Mihalas, D., & Mihalas, B. W. 1984, *Foundations of Radiation Hydrodynamics*, 1984 (Oxford: Oxford Univ. Press), 731  
 Molnar, M. E., Reardon, K. P., Chai, Y., et al. 2019, *ApJ*, **881**, 99  
 Morosin, R., de la Cruz Rodríguez, J., Díaz Baso, C. J., et al. 2022, *A&A*, **664**, A8  
 Park, H., Chae, J., Song, D., et al. 2013, *SoPh*, **288**, 105  
 Priest, E. 2014, *Magnetohydrodynamics of the Sun* (Cambridge: Cambridge Univ. Press), 2014  
 Socas-Navarro, H., & Uitenbroek, H. 2004, *ApJL*, **603**, L129  
 Souffrin, P. 1972, *A&A*, **17**, 458  
 Sych, R., & Nakariakov, V. M. 2014, *A&A*, **569**, A72  
 Tian, H., DeLuca, E., Reeves, K. K., et al. 2014, *ApJ*, **786**, 137  
 Yurchyshyn, V., Kilcik, A., Sahin, S., Abramenko, V., & Lim, E.-K. 2020, *ApJ*, **896**, 150  
 Zhao, J., Chen, R., Hartlep, T., et al. 2015, *ApJL*, **809**, L15